Earth's Climate and Weather: Dominant Variability and Disastrous Extremes Chapter 3: The Phanerozoic Climate

Nir J. Shaviv[1], Henrik Svensmark[2], Ján Veizer[3]

[1]Racah Institute of Physics, Hebrew University of Jerusalem, Jerusalem 91904, Israel
[2]National Space Institute, Technical University of Denmark, Elektrovej 327, 2800 Kgs. Lyngby, Denmark.
[3]Department of Earth and Environmental Sciences, University of Ottawa, Ottawa ON K1N 6N5, Canada

Key Points:

- Based on on lithological indicators of climate (e.g. coals, evaporites, tillites) and oxygen isotopic measurements, the Phanerozoic climate can be reconstructed, revealing regular changes between "icehouse" and "greenhouse" states.
- The dominant climate drivers over this period are the amounts of greenhouse gases in the atmosphere and atmospheric ionization governed by cosmic rays.

Abstract

The chapter reviews long-term climate variations during the last 540 million years (Phanerozoic Eon). It begins with a short review of the relevant geological and geochemical datasets available for reconstruction of the long-term climate variations. It then explores the main drivers of climate that appear to explain a large fraction of these climatic oscillations. The first is the long-term trend in atmospheric CO_2, due to geological processes, while the second is the atmospheric ionization due to the changing galactic environment. Other drivers, such as albedo variations and geographic effects, are of secondary importance. In this review we pay particular attention to problems that may affect the measurements of temperature obtained from oxygen isotopes, such as the long-term changes in the concentration of δ^{18}O seawater and the possible CO_2 biasing of it.

1 Introduction

Global climate change, on all time scales, is a fundamental aspect of Earth evolution. These climate variations have been caused by a range of drivers, which can be either intrinsic or extrinsic to the Earth's system. For example, on very long time scales, the solar output has slowly increased (Schwarzschild, 1958; Hoyle, 1958; Gough, 1981; Bahcall et al., 2001) giving rise to the so called young faint sun paradox (Ringwood, 1961; Sagan & Mullen, 1972; Ulrich, 1975; Pollack, 1991; Feulner, 2012). Simple stated, "If the Earth received less energy from the Sun in the early Precambrian, then why was the Earth so warm back then?". One suggested answer is that during the Precambrian the atmospheric composition gradually changed from a strongly reducing oxygen-deficient atmosphere with large amounts of greenhouse gases (such as CO_2, CH_4 and NH_3) to an oxygen-rich atmosphere with significantly lower concentrations of greenhouse gases. The greater concentration of greenhouse gases kept the Earth warm during the early Precambrian. Subsequently, the gradual

Corresponding author: Nir Shaviv, nir.shaviv@mail.huji.ac.il

increase in solar radiation was balanced by decreasing amounts of greenhouse gases (Sagan & Mullen, 1972; Kuhn & Kasting, 1983; Kasting, 1993; Feulner, 2012).

On much shorter time scales, we still find that global climate change is governed by intrinsic and extrinsic factors. For example, the eruption of Large Igneous Provinces (LIPS) can add massive amounts of greenhouse gases to the atmosphere which warm the Earth (Clapham & Renne, 2019), whereas bolide impacts can generally cool the Earth on both short (Chapman & Morrison, 1994; Pope et al., 1994) and intermediate time scales (Vellekoop et al., 2016).

Over very short time scales (20 to 100 ka), changes in Earth's orbital parameters, known as the Milankovitch cycles, affect the amount of insolation reaching high latitudes (Milankovitch, 1920; Köppen & Berlin, 1924; Hays et al., 1976; Berger, 1977). This in turn affects the growth or waning of ice-sheets that modulates the terrestrial energy budget by changing the Earth's albedo, thus impacting ocean temperature and global levels of atmospheric CO_2 (Pisias & Shackleton, 1984; Genthon et al., 1987; Imbrie et al., 1992; Ruddiman, 2006). Note, however, that Milankovitch's theory does have its caveats; the main one is related to the dominance of the 100 ka cycle. Consequently, alternative explanations were also suggested, such as the changes in Earth's orbital inclination (Muller, 1997).

Here, we shall concentrate on the "intermediate" time scale of 100's of millions of years and review climate change during the Phanerozoic Eon (Frakes et al., 1992; Veizer et al., 1999, 2000; Shaviv & Veizer, 2003; Veizer & Prokoph, 2015; Song et al., 2019; Vérard & Veizer, 2019; Scotese et al., 2021; Song et al., 2021; Goddéris et al., 2021). This is the time interval when complex life arose, producing numerous fossils that can be analyzed by chemical methods to describe global changes. The Phanerozoic is also characterized by a relatively stable atmospheric composition. We will review global climate change over this time scale, and show that the observed climatic variability is governed by a combination of both intrinsic and extrinsic drivers.

In this review we will not consider variations shorter than a few million years. As mentioned above, these are governed by orbital forcing, or by other short-term causes such as large scale volcanic eruptions or the out-gassing of methane from the deep sea as postulated, for example, for the Paleocene-Eocene Thermal Maximum – PETM (McInerney & Wing, 2011). We will also avoid discussion of regional drivers (e.g., climate change caused by the formation of mountain ranges, even if they may have a global effect) and will restrict our discussion to climate drivers on a global scale.

In part 2, we will review other models that describe how the global average temperature has changed during the Phanerozoic. These models are based on both geochemical and non-geochemical evidence and we will point out the advantages and problems with each method. We will then combine these estimates of paleotemperature to produce a more reliable Phanerozoic temperature curve which we will then explain in terms of the radiative drivers.

In part 3, we will review the principal intrinsic and extrinsic radiative drivers and explain how they affect the global temperature. The former, primarily greenhouse gases, vary due to geological activity (i.e., volcanic eruptions, chemical weathering). The latter include long-term variations in the solar output as well as changes in the galactic cosmic ray flux.

We will then continue, in part 4, to review the chronology of these climate drivers and in part 5 compare the predicted temperatures to the Phanerozoic paleotemperatures. We will demonstrate that the aforementioned intrinsic and extrinsic drivers can explain a significant portion of the observed temperature variations. Moreover, this comparison enables us to settle the protracted debate regarding the interpretation of ancient oxygen isotopic measurements of temperature. There is clearly a long-term,

secular drift in oxygen isotope values during the Phanerozoic which extends to the Archean, 3 billion years ago (Prokoph et al., 2008). Some authors claim that this trend is a result of post-depositional (diagenetic) recrystallization of samples that becomes more severe with their age (Grossman, 2012a, 2012b). Others (Veizer & Prokoph, 2015; Vérard & Veizer, 2019) argue that the trend reflects the evolving oxygen isotopic composition of sea water. This trend must be removed (i.e. detrended) to obtain realistic temperature measurements. See additional commentary below and in caption to Fig. 2.

This review is by no means comprehensive. Readers are directed to three additional reviews that have recently appeared on the topic of Phanerozoic paleotemperatures. Scotese et al. (2021) reviews Phanerozoic climate with an emphasis on lithologic indicators of climate. The second type of studies (Song et al., 2019, 2021) reviews the temperature record derived from oxygen isotope measurements obtained mostly from phosphatic, rather than carbonate, shells. The third review (Goddéris et al., 2021) combines observational data with climate models for the different Phanerozoic epochs. These reviews are all complementary to the discussion presented here. Our essay places an emphasis on modeling Phanerozoic climate as a whole, pinpointing the role of the main climate drivers, both intrinsic and extrinsic to the Earth's system, that operated continuously throughout the planetary history.

2 Reconstructing the Phanerozoic Climate

Generally speaking, there are two types of temperature and climate reconstructions over geological time scales. One type, based on lithological indicators of climate such as coals, evaporites, bauxites, and tillites (Frakes et al., 1992; Boucot et al., 2013) aim to reconstruct the Earth's past climatic zones (Köppen belts) and the pole-to-equator temperature gradient (Scotese et al., 2021). The second reconstruction is geochemical and uses oxygen isotope measurements of paleotemperature (Veizer et al., 1999; Grossman, 2012a, 2012b; Song et al., 2019; Vérard & Veizer, 2019). Both methodologies have important advantages and disadvantages.

2.1 Qualitative Lithological Proxies

Lithologic indicators of climate can be used to map the ancient climatic zones (Köppen belts). From the equator to the poles, the major Köppen belts are: 1. tropical rainforests, 2. desert belts, 3. warm temperate grasslands and forests, 4. seasonally warm/cold cool temperate regions, and 5. frigid polar regions. By mapping the ancient extent of these Köppen belts it is possible to estimate global average temperatures (Scotese et al., 2021).

Compared to the isotopic climate records described below, the downside of the lithological reconstruction of paleotemperature is that it is very hard to achieve high temporal resolution. The paleogeographic maps of Scotese and collaborators (Scotese, 2016, 2021) cover $\sim$ 100 slices of the Phanerozoic, with an average duration of $\sim$ 5 million years. On the other hand, it has one very clear and significant advantage. It does not suffer from any long-term secular biases that may affect the δ^{18}O data base, nor is it indirectly affected by any of the drivers themselves.

2.2 Quantitative Geochemical proxies

The shells of a variety organisms (brachiopods, foraminifera, mussels, conodonts) which live in diverse ecological environments are made of calcium carbonate, calcium phosphate and siliceous minerals. The ratio between the ^{18}O to ^{16}O isotopes found in these shells depends on multiple environmental factors. The primary factor is the temperature of the ambient water (Urey et al., 1951; Emiliani, 1954). The relationship

between δ^{18}O and temperature is such that a compositional change in δ^{18}O of -1‰ corresponds to about a $+4$°C increase in the temperature at the time of precipitation. However, the relation depends also on the salinity and the ratio of ^{18}O to ^{16}O in seawater. Salinity depends on paleoclimate (arid vs humid climates), and the ratio of ^{18}O to ^{16}O in seawater depends in part on the amount of water locked in the continental ice caps. For example, assuming that during glacial maximums the amount of water locked in continental ice is about twice the volume of the Antarctic ice cap ($\sim$ 30 million km^3) and that no polar ice caps existed during warm intervals, the expected variations from waxing and waning of ice caps would be about 2‰ (Veizer et al., 2000).

While the δ^{18}O reconstruction has a clear advantage in providing quantitative, high resolution data (with appropriate environmental corrections), there are three major caveats that must be taken into account.

Quite early on, it was realized that there is a 4-8‰ decline in δ^{18}O for progressively older Phanerozoic measurements (Baertschi, 1957; Clayton & Degens, 1959), and double that for the early Precambrian (Prokoph et al., 2008). If taken at face value, it would imply unrealistically high ocean temperatures of 30°C during the extensive Ordovician/Silurian glaciations, 50°C during the late Cambrian (Song et al., 2019, and figure 1), and almost near boiling oceans during the Precambrian, even at times of massive glaciations (Kopp et al., 2005). The general wisdom for the last four decades therefore implied that a diagenetic process superimposed itself over temperature fractionation (Grossman, 2012a, 2012b), making the data useless for long time scale temperature reconstruction. This changed with Veizer et al. (1999), who compiled thousands of oxygen isotope measurements of well-preserved low-Mg calcitic fossils over the entire Phanerozoic. They documented a clear cyclic pattern of oscillations superimposed on a secular trend that was consistent with climate variations deduced from lithological indicators, demonstrating that the original temperature imprint remained in the fossils. It should be noted, that the same samples yielded also additional measurements that were entirely consistent with independent studies of other laboratories, such as isotopes of carbon and radiogenic strontium (Veizer et al., 1999), stable strontium (Vollstaedt et al., 2014), sulfur (Kampschulte & Strauss, 2004), calcium (Farkaš et al., 2007), and Sr/Ca elemental ratios (Steuber & Veizer, 2002). It is difficult to argue that oxygen, the dominant element in the calcite structural cell was completely, diagenetically, replaced while all other major and minor elements and isotopes remained untouched. Moreover, the long-term secular trend was documented not only for carbonates, but also for siliceous and phosphatic samples. These isotopic changes cannot be therefore explained in terms of diagenesis because these three mineral phases differ in their stability and their isotopic fractionation factors. Their time series records, such as the ones discussed later in Fig. 2, would then show divergent trends, in response to variable sensitivity to resetting processes. The long-term secular trend is more likely primary, reflecting a non-monotonous slow (of order 0.01‰/Ma) oxygen isotopic evolution of sea water, possibly due to the slowing of the plate tectonics which buffers the oceanic δ^{18}O (Vérard & Veizer, 2019).

The second caveat is more delicate. Zeebe (1999) pointed out that ocean acidity can produce an offset in the δ^{18}O data that mimics temperature variation: $\Delta T_{\mathrm{pH}} = bs\Delta\mathrm{pH}$ with b being the ratio between oxygen fractionation and temperature, i.e., $b \sim 4$°C per ‰, and s being the ratio between δ^{18}O and pH variations, which from theory and experiments appears to be around $s = -1.42$‰ per unit pH (Zeebe, 2001). Royer et al. (2004) then suggested that the Phanerozoic temperature reconstruction would be affected by the atmospheric concentration of CO_2 which modifies oceanic acidity. The implication was that part of the temperature response to CO_2 warming is countered by corresponding pH variations. In fact, for the canonical values used by Royer et al. (2004), it was shown by Shaviv (2005) that for a climate sensitivity of ~ 1.5°C increase per CO_2 doubling, there should actually be no correlation between the δ^{18}O derived

temperature and the CO_2. This could explain the lack of correlation between CO_2 and temperature found in Veizer et al. (2000), Shaviv and Veizer (2003) and Davis (2017). Note also that the scenario of Royer et al. (2004) involves multiple assumptions about processes that relate ocean acidity and alkalinity to pCO_2. These assumptions should be taken with a grain of salt. In the following sections we will try to estimate this bias empirically, by comparing the lithological and isotopic reconstructions of paleotemperature. We define the "unbiased" temperature as the real temperature while the "biased" temperature is the one modified through the pH bias.

The third caveat relates to the fact that most fossils producing hard mineral shells lived in tropical and warm temperate habitats ($< 40^\circ$ latitude). The Phanerozoic oxygen isotope temperature record therefore reflects the temperature of low latitude seas rather than the entire global ocean (see Scotese et al., 2021, for a detailed discussion of the issue and scaling).

2.3 A Combined Temperature Reconstruction

Given that the caveats of the different types of data sets are entirely independent, one could, in principle, combine lithological and geochemical data into a new temperature reconstruction that avoids the aforementioned problems. This was realized by Scotese et al. (2021), who generated a Phanerozoic temperature reconstruction that is based on both lithological indicators of climate on long time scales and oxygen isotope data on the intermediate 10-20 my time scales. Interestingly, Scotese et al. (2021) compared their Phanerozoic temperature model to short-term LIP eruptions and bolides impacts, finding that 19 of 21 LIP eruptions broadly match the times of elevated temperatures, while 18 of 22 of the major bolide impacts correspond to the times of global cooling. In this essay, we combine the same lithological and geochemical data sets (Figure 1) using a different technique, described below, while considering that some of the proxy data can be systematically biased. We obtain a similar result (Figure 2).

If we define a smoothing kernel, $K(t,t') = \left(1/\sqrt{2\pi}\sigma_t\right)\exp\left(-(t-t')^2/(2\sigma_t^2)\right)$, with σ_t taken to be 30 million years, we can combine Scotese et al. (2021)'s lithological reconstruction T_L with Song et al. (2019)'s isotopic reconstruction T_I (Fig. 1 as follows:

$$T_C = \int_{-\infty}^{\infty} K(t,t')T_L dt' + \left(T_I - \int_{-\infty}^{\infty} K(t,t')T_I dt'\right). \tag{1}$$

This definition recovers T_I for $\sigma_t \to \infty$ and T_L for $\sigma_t \to 0$. In order to avoid edge effects, we carry out the integral from 0 to $t_{\max}$, normalize K appropriately and correct for the asymmetric boundaries by fitting a linear slope and correcting the expected bias in the integral.

Fig. 2 compares our combined temperature reconstruction (this study, solid line) with the Scotese combined model (dashed line). Both curves use the same input data T_I and T_C. The differences between the two curves are due to the fact that Scotese et al. (2021): 1) used a σ of 55 million years, which reduced the overall amplitude of the curve, 2) employed the Savitsky-Golay fitting technique to smooth the curve, and, 3) modified the curve to better agree with geological and paleontological constrains (most notably at 30 Ma, 66 Ma, 310 Ma, and 340 Ma). The difference between original non-detrended isotope data of Song et al. (2019) and our combined reconstruction that effectively detrends the isotopic data, is plotted as the dash-dotted curve in Fig. 2.

Our base temperature reconstruction ("this study") will serve as the data we will analyze below. It can also be found at `http://www.phys.huji.ac.il/~shaviv/the-phanerozoic-climate`.

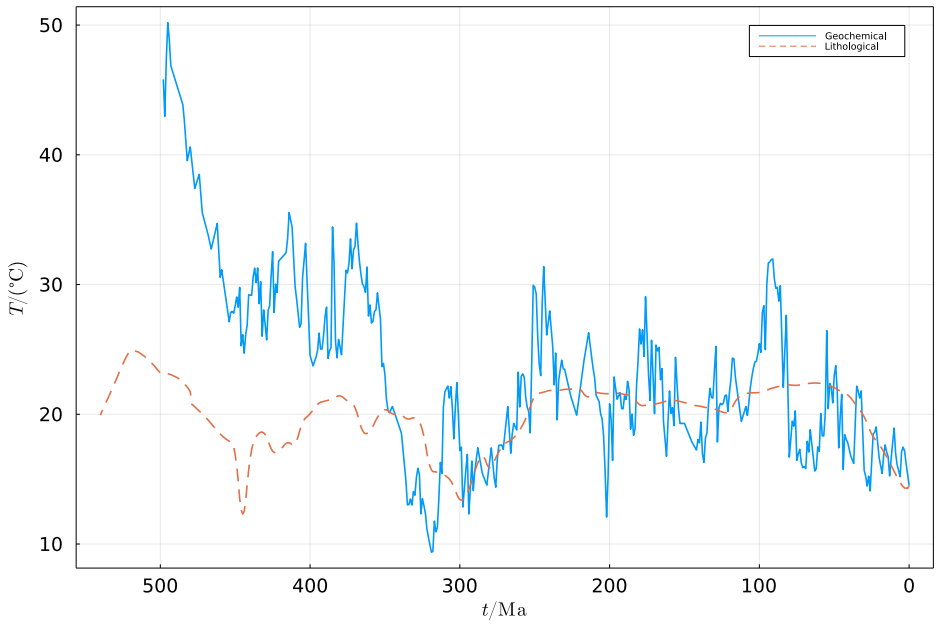

Figure 1. The underlying reconstructions used in the present analysis. The geochemical reconstruction (Song et al., 2019) is depicted with a solid line, while the lithological reconstruction (Scotese et al., 2021) is dashed. Note that whereas some of the gross features are similar, a notable difference is the extreme geochemically based reconstructed temperatures derived for the early Phanerozoic.

3 Main Climate Drivers of the Phanerozoic

The climate drivers over the Phanerozoic can be divided into two primary groups. The first is drivers intrinsic to the Earth system, the variation of which arises due to various geological processes. The second is extrinsic drivers which depend on Earth's interaction with its celestial environment.

3.1 Intrinsic Drivers - Atmospheric Composition

By far, the most important intrinsic climate driver is the changing atmospheric composition. Triatomic (or larger) molecules have absorption bands in the infrared (IR) that give rise to the so-called Greenhouse effect. Increasing their atmospheric abundance increases the IR optical depth such that the surface from which the terrestrial radiation can be radiated back to space is generally higher in the atmosphere. Below this surface, a temperature gradient has to exist to advect the heat from the surface (either through convection or radiation) to the height from which the IR is emitted to space. Thus, increasing the amount of Greenhouse gases implies that the temperature gradient has to exist over a larger height and the surface temperature therefore has to increase.

The most abundant triatomic molecule is that of water. However, because it is condensable it cannot be considered as a climate driver, since the amount in the atmosphere is the result of a climate equilibrium, not due to extrinsic processes. The next triatomic (or more complex) molecule in the atmosphere is CO_2. Although some of the processes depend on the temperature (equilibrium between atmospheric CO_2 and mostly carbonic acid in the oceans), the large variations over geological times scales

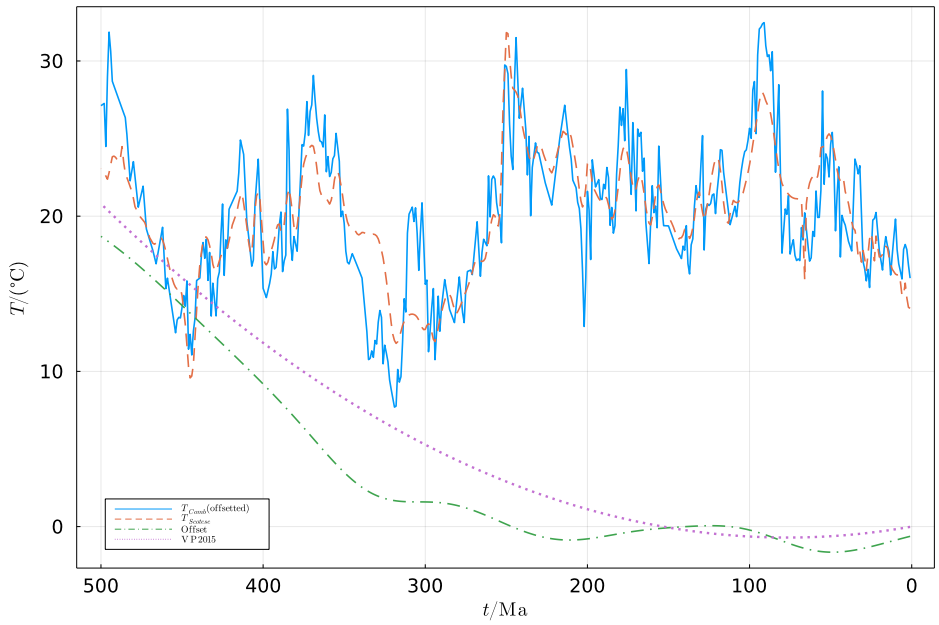

Figure 2. Scotese et al. (2021) reconstruction (dashed) is based on lithological data on long time scales and oxygen isotope data for medium time scales (10-20 Ma). The lithological/geochemical combined reconstruction we use here (i.e., eq. 1), is in solid line. The difference between the non-detrended isotopic reconstruction of Song et al. (2019) and our combined reconstruction is plotted with a dash-dotted line. It depicts the systematic secular offset in isotope data discussed above. Without this correction the data taken at face value would require unrealistically hot temperatures (i.e., Song et al., 2019) for the ancient oceans. Note that the systematic correction of -4°C per 1‰ δ^{18}O suggested by Veizer and Prokoph (2015) for oxygen isotope record of carbonate shells (dotted) is practically identical to the one employed here and based mostly on phosphatic shells.

depend on geological processes and not temperature (mostly volcanic activity vs. sedimentation as limestone). The effect of the greenhouse gases is usually quantified as the change in radiative forcing associated with an increase in their atmospheric abundance, in other words, how does the radiation to space change if we increase or decrease amount of greenhouse gases but do not change the thermal profile of the atmosphere. Since the infra-red radiative lines are mostly saturated, the differential contribution is from the line wings such that an increase in the amount of the greenhouse gases generally increases the radiative forcing only logarithmically. It is therefore customary to define the greenhouse effect as the change in radiative forcing associated with doubling in the concentration of greenhouse gases. For CO_2, the standard estimate for the radiative forcing associated with a doubling of CO_2 is $\Delta F_{\times 2} \approx 3.7 \mathrm{W/m^2}$ (Myhre et al., 1998). Other greenhouse molecules that have made a contribution over geological time scales are methane and ammonia. However, beyond direct measurements in ice-cores in the past million years, there is no reliable way to estimate their past atmospheric concentrations.

Other effects on the radiative budget arise from changes in the Earth's albedo. These include changes in the surface albedo (due to ice and vegetation) and due to cloud cover. One can roughly estimate the surface albedo (in particular, the contribution from ice). However, we don't consider cloud cover variations to be a climate driver

(except perhaps through cosmic rays as explained below), but instead they are part of how the climate reacts to imposed drivers. Since we will not estimate the albedo effects, it will imply that any albedo effects that are due to a response of the terrestrial system to climate changes, such as the extent of glaciations, are going to be implicitly considered to be part of the overall climate sensitivity which we describe below.

Other climate drivers include a changing geography, such as mountain ranges that affect air mass flow, or changes in oceanic circulation. It is hard however to assess the effects of such drivers on a global scale, let alone reconstruct them over geological time scales. We will therefore omit discussing them altogether. Unlike the albedo response to the climate, we do not expect these drivers to be climate-driven. Ignoring the climatic effects of changing geography implies that some of the observed climate variations are left unexplained.

3.2 Extrinsic Drivers - Solar output and cosmic rays

Perhaps the best known extrinsic driver are Milankovitch cycles in which the gravitational forces exerted by the sun, moon and planets effect the orbital parameters of the Earth. Milankovitch cycles give rise to climate variations on a timescale of 20 to 100 kyr and therefore, are irrelevant when considering climate change on the timescale of the Phanerozoic (10's of millions of years).

There is however another extrinsic driver that acts on time scales of millions of years. Although the idea has been controversial, we now know that cosmic ray flux (CRF) variations have a large effect on the climate. They were first considered as the mechanism linking solar variations to terrestrial climate (Svensmark & Friis-Christensen, 1997), but later it was realized that they can explain climate variations over geological time scales as well (Shaviv, 2002, 2003a; Shaviv & Veizer, 2003; ?, ?). With the exception of cosmic rays with extremely high energies, most cosmic rays (CRs) are high energy particles that are accelerated in supernova remnants. They then diffuse through out the Milky Way (typically 10 Ma), eventually escaping the galaxy. Those cosmic rays that reach the solar system are slowed down by the solar wind, but once they reach Earth's atmosphere, they generate charged particle showers that reach the lower troposphere. Cosmic rays are the dominant source of atmospheric ions. Interestingly, the flux reaching the earth's surface decreases when solar activity is on the rise. Cosmic ray production also varies according to the production rate in the solar system's vicinity.

Today we know that this atmospheric ionization plays an important role in the nucleation of the few nannometer (nm) sized aerosols, called condensation nuclei (Svensmark et al., 2007; Enghoff & Svensmark, 2008; Kirkby et al., 2011), and in their growth to the $\sim$ 50 nm sized aerosols called cloud condensation nuclei - CCNs (Svensmark et al., 2013; Svensmark et al., 2017). These processes have been described analytically from ab initio physical principles; they have been observed in the lab, and they also have been seen to operate empirically in situ. A few examples include:

1. Forbush decreases. It is possible to decouple CRF variations from other changes related to the solar activity (such as UV) over the time scale of days and record the physical chain of events that consequently takes place between atmospheric ionization changes and CCNs. Forbush decreases are several day long reductions in the CRF which appear typically one day after large eruptions on the solar surface. The strongest Forbush decreases are associated with reductions in the number of aerosols, as well as with changes in different cloud parameters derived from cloud data sets and satellites (Svensmark et al., 2009, 2016).
2. Although the 11-year cycle in the cloud cover could, in principle, arise from another solar link, one which is unrelated to the cosmic ray flux, the observed

cloud cover changes have a cosmic ray imprint in them. The 11-year cycle is actually a 22-year cycle. Every 11-years, the north and south magnetic poles of the sun flip. It turns out, however, that only the cosmic rays are sensitive to the polarity switch. This sensitivity manifests itself as an asymmetry between odd and even solar cycles—the cosmic ray minimum is flat during one cycle, and becomes more pronounced during the next. Other variations such as the UV flux or the strength of the magnetic field are not affected by the magnetic polarity. It is notable that changes in cloud cover exhibits the same asymmetry as cosmic rays (Fichtner et al., 2006).

3. The cosmic ray / climate relationship is the only one capable of explaining the magnitude of the observed solar-climate interactions. For example, though it has been suggested that UV heating the stratosphere may be the result of increases in solar activity, (Haigh, 1994) global circulation models show that the net effect on the surface temperature is actually less than the variations due to the changed irradiance (Lee & Smith, 2003; Haigh et al., 2005). On the other hand, the apparent effect that the cosmic rays have on cloud cover automatically explains the size of all the observed solar-related climate variations. For example, the changes in the energy budget associated with the 11-year cloud cover variations have the right amplitude to explain the calorimetric measurement of the solar radiative forcing (Shaviv, 2008; Howard et al., 2015).
4. Over geological time scales, there are large variations in the cosmic ray flux which have nothing to do with solar variability. Instead, they arise from the movement of the solar system through different galactic environments. A comparison between the cosmic ray flux (reconstructed over these time scales using iron meteorites) and climate (reconstructed using either sedimentation or geochemical records) demonstrates that the seven ice-age epochs (during which Earth has had glaciations) over the past billion years have taken place when the cosmic ray flux was higher, as the theory predicts (Shaviv, 2002; Shaviv & Veizer, 2003; Shaviv, 2003a). Over somewhat shorter time scales, one can also see 15 time periods when the solar system oscillates perpendicular through the galactic plane (?, ?). We will consider these variations in the discussion that follows. On longer time scales, the secular decrease of the solar wind may explain part of the faint sun paradox, and long term star formation variations in the Milky Way may also explain why glaciations are seen only during the Phanerozoic, Neo-Proterozoic and the late Archean-Huronian. These variations can be reconstructed from the age distribution of nearby stars. They may arise from tidal perturbations during perigalacticons of the Large Magellanic Cloud, and are a natural consequence of the cosmic ray climate link as a larger star formation rate will translate to more nearby supernovae (Shaviv, 2003b).

Another very important extrinsic climate driver is the slow increase in the solar luminosity. Insolation steadily increases because the average chemical weight at the solar core increases as hydrogen is fused into helium. As mentioned previously, this long-term change in insolation has given rise to the so called "faint sun paradox", i.e., how could Earth remain mostly unfrozen during most of its existence, even though the sun was much fainter in the distant past. Over the past 600 Ma, it corresponds to a 5% increase in solar radiation (Bahcall et al., 2001). It is perhaps the easiest driver to consider.

3.3 Climate Sensitivity

To the extent that we can describe the climate with a single number—the average global temperature—the climate sensitivity links this number to the change in the radiative forcing. If earth were a perfect gray body (that is, a black body in the IR with constant emissivity but "gray" with a finite constant albedo in the visible),

then comparison of the shortwave flux entering the system, $\pi R^2(1-a)S_0$ (with a, R, and S_0 being the albedo, Earth's radius and Solar constant) to the infrared leaving it $4\pi R^2 \epsilon \sigma T^4$ (with ϵ, σ and T being the IR emissivity, Stephan-Boltzmann constant, and an effective temperature describing Earth), then Earth's equilibrium effective temperature would be

$$T = \left(\frac{(1-a)S_0}{4\epsilon\sigma} \right)^{1/4}. \tag{2}$$

The climate system is however much more complicated because positive feedback changes both the albedo, a, and the emissivity, ϵ, in the above equation. For example, cooling the planet would increase the extent of ice cover, thus increasing the albedo and further cooling the planet. Increasing the average global temperature would increase the amount of water vapor in the atmosphere, but it would also change the cloud cover - further affecting both a and ϵ. Thus, it is extremely hard to calculated Earth's climate sensitivity ab initio. The canonical range set more than 4 decades ago (Charney Committee, 1979) is that doubling the amount of CO_2 should increase the temperature by 1.5 to 4.5°C. This is also the range indicated in the IPCC scientific reports (IPCC, 2013). However, climate simulations have a very hard time pinning down this number because of the large uncertainties in the feedbacks, especially through changes in the cloud cover.

4 Reconstructing Phanerozoic climate drivers

Once we characterized the main drivers and how they affect the climate, the next step is to reconstruct their variations over the Phanerozoic.

4.1 Reconstructing the Atmosphere

The standard yardstick for pCO_2 temperature reconstruction is the GEOCARB model (Berner, 2001), later expanded in the GEOCARB-SULF model to describe the carbon, sulfur and oxygen cycles (Berner, 2006; Royer et al., 2014). The model includes several dozen parameters and integrates various proxy measurements of CO_2. Other greenhouse gases, such as methane or ammonia are significantly less constrained, either theoretically or through observations. On a multi-thousand year time scale, atmospheric concentration CO_2 and CH_4 can be directly measured from ice-cores, but over the Phanerozoic the concentration of CO_2 must be reconstructed from a variety of proxies, each with a large degree of uncertainty (Royer et al., 2014). Nonetheless, there is a very clear correlation between CO_2 and CH_4 levels observed in ice-cores, such that the total radiative forcing of both gases is about 20% larger than CO_2 alone. If similar correlations exist over the Phanerozoic time scale as well, then it would introduce biases that might be difficult to unravel. More about it in the discussion below. All things considered, this implies that we are left with a large uncertainty regarding the drivers of atmospheric radiation.

4.2 Solar luminosity increase

The solar luminosity increase is relatively straightforward to reconstruct. It is based on well tested solar models satisfying very stringent constraints on the luminosity today, surface abundances and helioseismology observations. Gough (1981) has shown that the solar luminosity at time t before present can be written to a very good approximation as $L(t)/L_\odot = (1 + 0.4t/t_\odot)$, with t being the time relative to today (which is negative in the past), and $t_\odot = 4.57$ Ga, except for the first 200 Ma of the solar system's life. This was corroborated by Bahcall et al. (2001) who found a 5% linear increase over the past 600 Ma.

4.3 Reconstructing cosmic ray flux variations

Once meteorites break off their parent body, their surfaces interact with cosmic rays producing spallation products. Some of these products are radioactive, while others are stable. The ratio between the two spallation products provides the integrated cosmic ray flux that the meteorite was exposed to between its formation and its penetration into Earth's atmosphere. The standard assumption is that the CRF is roughly constant such that the integrated flux corresponds to the *exposure age* of the meteorite. This assumption, however leads to an inconsistency between exposure ages derived from "short lived" radionucleotides, such as ^{10}Be and exposure ages based on ^{40}K with a half life of 1.25 Ga. This led to the conclusion that the cosmic ray flux (CRF) must vary over geological time scales, being about 30% higher over the past few Ma than its average over the past 1 Ga (Lavielle et al., 1999).

It was then proposed that the exposure age of meteorites can actually be used to reconstruct the CRF history (Shaviv, 2002, 2003a). If one assumes, statistically, that meteorites are produced at roughly a constant rate, then the distribution of their exposure-ages provides an estimate of the time varying CRF. It was found that the CRF exhibits a 145 Ma oscillation over the past 1000 Ma. Given that there are very few older iron meteorites, it is impossible to extend the CRF reconstruction further in time using this approach. Also, the limited number of iron meteorites and the relatively few exposure age determinations means that age estimates finer than a few 10 Ma are not possible. Shaviv (2003a) has shown that the ∼145 Ma periodicity in CRF corresponds to passage of the solar system through one of the two sets of spiral arms of the Milky Way (a 4-armed set that extends from our galactocentric radius outwards, and which is rotating at roughly half the angular speed that the solar system does).

To reconstruct the variations of CRF on other time scales, it is necessary to resort to theory. On the several 10's millions of year time scale, we expect CRF variations to arise from the vertical oscillation of the solar system perpendicular to the galactic plane. Observations of the kinematics of A and F stars (which have an intermediate age, sufficient to have reached kinematic equilibrium in the galactic potential perpendicular to the disk, but not too old to be too faint or to have strayed to large vertical distances), give a half crossing period of typically 30-45 Ma (Bahcall & Bahcall, 1985; Stothers, 1998; Holmberg & Flynn, 2000). The problem however is that such kinematic methods suffer from a large systematic bias arising from the spiral arm shocks perturbing the distribution of the stellar velocities during each spiral arm passage (Shaviv, 2016). Thus, we do not have independent CRF reconstructions arising from the vertical motion. Nonetheless, we do have two consistency checks which the paleoclimate temperature reconstruction should satisfy. Apart from a rough range of periods, the phase should be close to peak coldness given our location close to the galactic plane. Moreover, a secondary oscillation arising from the radial epicyclic motion of the solar system, having a period of typically 180 Ma, should manifest itself as an oscillation in the period of the vertical oscillation. Both consistency checks are satisfied by the data (?, ?).

5 Comparing the drivers to the climate

Armed with the Phanerozoic temperature reconstructions (Scotese et al., 2021, this study, see Figure 1) which minimize the problems of either the lithological or the geochemical data, we can now compare it to the climate drivers. To do so, we use a model which parametrizes the drivers and the temperature reconstructions, while considering the uncertainties. The predicted model temperature assumes greenhouse forcing by CO_2, heating by the slowly brightening sun, as well as two oscillatory components that describe the effects of spiral arm passages and the vertical motion of the solar system. We also assume that the geochemically measured temperature has

a bias through the aforementioned pH alteration of δ^{18}O. Thus, we write

$$\begin{aligned} T_{pred} &= T_0 + \Delta T_{\times 2} \log_2(\mathrm{pCO_2/p_0}) - \alpha \Delta T_{\times 2} R_L t \\ &\quad + \frac{A_l}{2} \cos\left(2\pi t/P_l - \phi_l\right) \\ &\quad + \frac{A_s}{2} \cos\left((2\pi/P_l)\left(t + A_{2nd}/2\cos(2\pi t/P_{2nd} - \phi_{2nd})\right) - \phi_l\right) \quad (3) \\ T_{biased} &= T_{pred} + \Delta T_{bias} \log_2(\mathrm{pCO_{2,fast}/p_0}). \quad (4) \end{aligned}$$

T_0 is the temperature for the fiducial parameters of the forcing. $\Delta T_{\times 2}$ is the global temperature increase per CO_2 doubling. p_0 is the preindustrial atmospheric concentration. R_L is the rate with which the solar radiative forcing increases. α is the ratio between the sensitivity to solar forcing and CO_2. Naively one would expect this number to be unity, however, various additional effects could enter. A_l and A_s are the peak to peak amplitudes of the long term and short term oscillations (presumably due to spiral arm passages and oscillations perpendicular to the galactic plane). P_i, ϕ_i are oscillation period and phase. Note that the short term oscillation also includes a phase oscillation. T_{biased} is the biased temperature, and it depends on ΔT_{bias} which is also a free parameter.

The analysis methodology is as follows: 1. We first generate a combined temperature reconstruction as described in part 2.3. 2. For a given set of model parameters, we predict an unbiased and a CO_2/pH biased temporal curves for the temperature. 3. We then find the model parameters which minimize the χ^2 difference between the model temperature and reconstructed temperature curve. The minimization procedure uses a combination of simulated annealing to scan the parameter space for minimums to find the global one, and then uses the steepest gradient method to accurately pin point the minimum. 4. For the error analysis we use the bootstrap method. We degrade the data by randomly discarding 1/e of the data and repeating the reconstruction and then the minimization procedure. For the high resolution geochemical data (Song et al., 2019), we assume each 1 Ma data point is uncorrelated. For the geochemical/lithological reconstruction we use 15 Ma bins. 5. The fit procedure is independently carried out to the Scotese geochemical/lithological temperature curve (dashed curve, Figure 2) curve, and to the lithological/geochemical temperature curve of this study (black curve, Figure 2). The results are summarized in table 1.

The first outcome of the table is that the fit to the lithological/geochemical temperature curve of this study yields model parameters that are similar to the fit for the Scotese temperature curve, though the results of this study have generally smaller errors. The last column of the table quantifies the significance of the derived model parameters arising from the lithological/geochemical temperature curve of this study. Clearly then, we find statistically significant signatures to the CO_2 radiative forcing (at 7.6σ), as well as to the periodic signals associated with the spiral arm passages (at 16.7σ) and to the vertical oscillation of the solar system (at almost 7.9σ).

The results are also depicted in figures 3-5. Figure 3 depicts the two temperature constructions (Scotese et al., 2021, and this study) as well as the model fit (Figure 3, gray dash-dotted line). It is evident from Figure that the three climate drivers used in the model (i.e., CO_2 radiative forcing (dash double dotted line), atmospheric ionization (dashed line), and solar luminosity (black dash dotted line) explain most of the temperature variations observed during the Phanerozoic, at least on time scales longer than $\sim$ 10 million years.

Figure 4 depicts 2D probability distribution functions for a few parameter pairs when the rest are marginalized. The first three pairs are the amplitude and period of the long and the short oscillations, and the secondary phase modulation of the short oscillation. The dashed lines correspond to the fit to the Scotese model while the colored contours correspond to the fit to the combined data of this study. The

Parameter	Meaning	Scotese Model	Present Model	Signific.
$\Delta T_{\times 2}$	Sensitivity to CO_2 doubling	$1.52 \pm 0.3°C$	$1.67 \pm 0.22°C$	7.6σ
λ	Sensitivity to solar flux	$0.96 \pm 0.09°C\ W^{-1}m^{-2}$	$0.89 \pm 0.16°C\ W^{-1}m^{-2}$	10.2σ
α	Solar warming to CO_2 ratio	1.95 ± 0.25	1.91 ± 0.12	
$\Delta T_{\rm bias}$	Indirect CO_2 bias of $\delta^{18}O$	–	-0.07 ± 0.62	
A_{long}	Large oscillation / amp.	$7.2 \pm 0.8°C$	$6.8 \pm 0.4°C$	16.7σ
P_{long}	Large oscillation / period	140.2 ± 1.7 Ma	140.0 ± 0.8 Ma	
ϕ_{long}	Large oscillation / phase	$214 \pm 9°$	$220 \pm 5°$	
A_{short}	Short oscillation / amp.	$2.6 \pm 0.4°C$	$2.6 \pm 0.3°C$	7.9σ
P_{short}	Short oscillation / period	32.7 ± 0.8 Ma	30.7 ± 0.7 Ma	
ϕ_{short}	Short oscillation / phase	$203 \pm 50°$	$117 \pm 40°$	
A_{2nd}	Secondary oscillation / amp.	$18.4 \pm 8°C$	$21.6 \pm 7°C$	3.0σ
P_{2nd}	Secondary oscillation / period	181.5 ± 6 Ma	175 ± 3 Ma	
ϕ_{2nd}	Secondary oscillation / phase	$80 \pm 48°$	$66 \pm 61°$	
A_{2nd}	Short oscillation / total amp.	$18.4 \pm 8°C$	$21.6 \pm 7°C$	3.0σ
P_{2nd}	Short oscillation / period	181.5 ± 6 Ma	175 ± 3 Ma	
ϕ_{2nd}	Short oscillation / phase	$80 \pm 48°$	$66 \pm 61°$	

Table 1. Model Parameters fitting the Phanerozoic. Errors are 1 σ ranges.

last pair describes the solar forcing sensitivity and the sensitivity to CO_2 doubling. Because the long-term decrease in CO_2 mostly cancels the increasing solar luminosity, they should have a linear relation, giving the narrow oval contours. The finite length of these contours arises from the fact that the CO_2 is not entirely monotonic such that its contribution can be fingerprinted.

Because the long-term decrease in CO_2 should mostly offset the increase in the solar luminosity, given that both temperature curves do not exhibit any net temperature trend over the entire Phanerozoic, one can relate the CO_2 forcing in terms of the changing solar luminosity. Since the solar luminosity increase is very well determined from solar evolution models, we can quantify the CO_2 forcing. This is depicted in the left panel of fig. 5. We find that the CO_2 should be $2.1 \pm 0.1 W/m^2$ per CO_2 doubling. This should be compared with the $3.7 W/m^2$ per CO_2 doubling obtained from radiative transfer models (Myhre et al., 1998), suggesting perhaps that the CO_2 has a radiative forcing which is smaller than expected, or that there are unaccounted systematic errors.

The right panel of fig. 5 depicts the quantification of the possible bias in the geochemical data, which arises from the $CO_2 \rightarrow$ pH $\rightarrow \delta^{18}O$ link. We find no appreciable bias which would imply that the oceans have had a relatively strong buffering effect to the pH variable.

6 Discussion and Summary

In part 2 we discussed a novel type of temperature record that combines lithological evidence of climate with geochemical ($\delta^{18}O$) temperature measurements. There are distinct advantages to this combined approach because the data sets are completely independent of each other and therefore, the errors are orthogonal. The temporal resolution of lithologically-based paleo-Köppen belts is poor, however, these reconstruc-

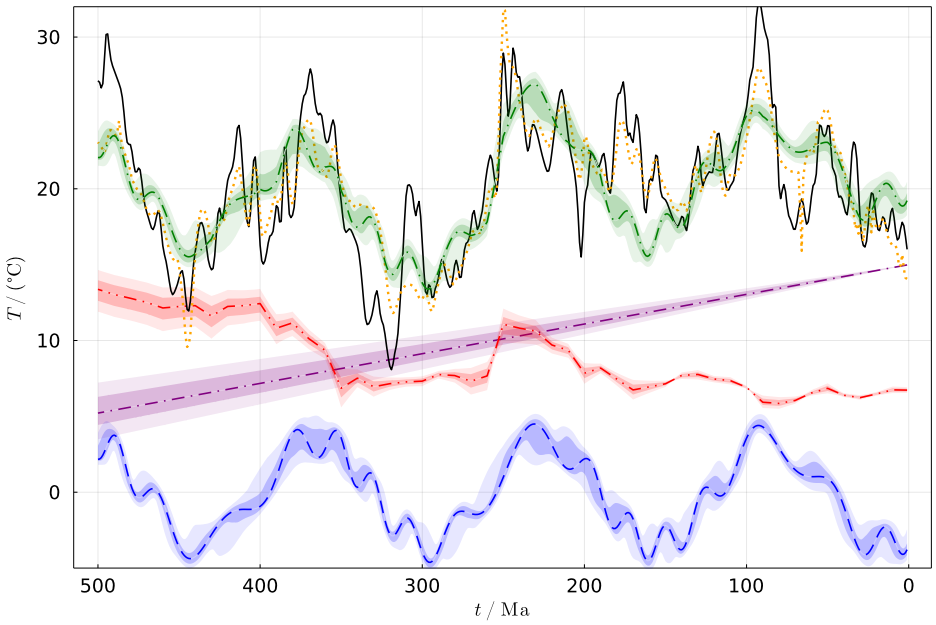

Figure 3. Phanerozoic average global temperature. Plotted are the geochemical/lithological reconstruction of Scotese et al. (2021) (dotted) and combined goechemical/lithological reconstruction (this study, solid), as well as the modeled temperature (dash-dot, gray). The additional graphs are the different components in the model - atmospheric ionization (bottom, dashed), CO_2 (dash double dot) and increasing solar luminosity (dash-dot gray). The shaded regions are 1-σ and 95% confidence error regions.

tions are immune to certain systematic biases that exist in the geochemical records. The first is the long-term drift in the baseline δ^{18}O–temperature calibration. The second is the fact that δ^{18}O can, in principle, depend on the atmospheric CO_2 levels (through the effects of ocean acidity), implying that $pCO_2 \rightarrow \Delta T \rightarrow \delta^{18}O$ may not be the only route affecting the isotopic record. By combining the best attributes of both methodologies, it is possible to produce a hybrid data set that can overcome these problems. Guided by the long term lithological record, it relies on the δ^{18}O record to provide the short term variations (Scotese et al., 2021).

We also reviewed the major global climate drivers that appear to operate over the Phanerozoic. These include drivers that are intrinsic to the Earth's system, and drivers that are extrinsic to it. We expect the former group to include several drivers, such as greenhouse gases, changing continental distribution, albedo variations and more. However, the only driver we can reliably estimate when modeling Phanerozoic temperature is CO_2. As for the other drivers, some may be important, but they are either difficult to reconstruct (such as other greenhouse gases), or their global effect is difficult to assess quantitatively (such as changing continental geography). In the best-case scenario, some of the temperature variations are left unexplained. The more problematic scenario involves drivers that may correlate with CO_2. For example, CH_4 correlates with CO_2 in the ice-core based records over the past several hundred thousand years; as a result the overall CO_2 forcing is effectively increased by about 20%. Such a correlation over the Phanerozoic would give rise to systematic errors that would affect the conclusions described below.

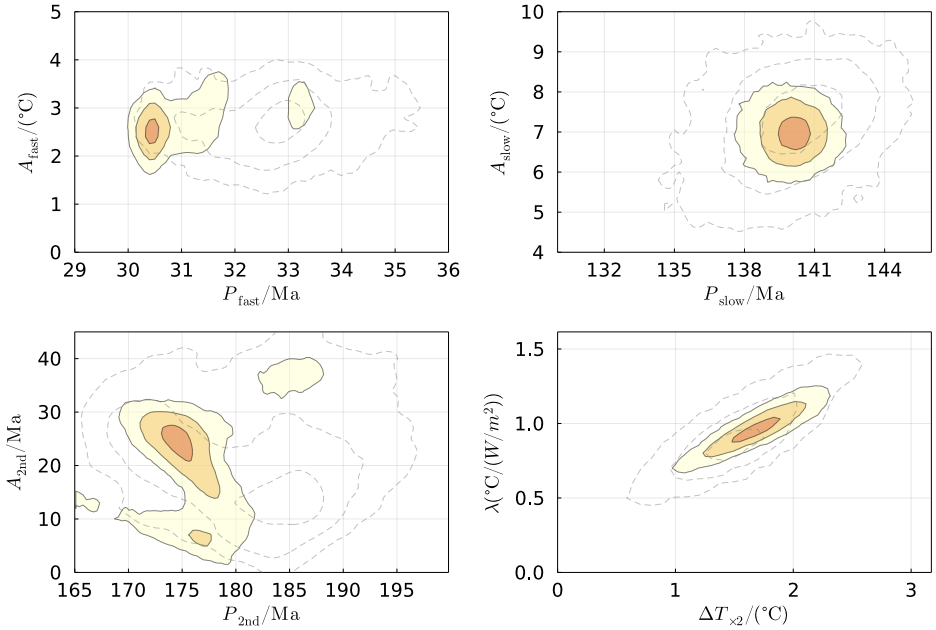

Figure 4. Distribution of model parameter pairs, when the rest are marginalized. Dashed and shaded contours are based on the Scotese model and combined data of this study respectively. Top left: The amplitude and period of the fast oscillation (presumably the vertical motion of the solar system), Top right: The amplitude and period of the slow oscillation (presumably the spiral arm passages). Bottom left: The amplitude and period of the secondary period modulation of the fast oscillation (Presumably due to radial epyciclic motion of the solar system in the galaxy). Bottom right: $\Delta T_{\times 2}$ - the climate sensitivity to changes in CO_2, and α - the sensitivity factor of the climate to the solar luminosity increase (see text).

Besides the intrinsic factors, we also expect extrinsic factors to influence Earth's climate as well. On "short" time scales it is the Milankovitch cycles, which, however, are too rapid to be seen on the time scales employed in this study (i.e., millions of years). However, we expect the slowly changing galactic geography to have had an effect on the Earth's climate through modulation of ionization in the Earth's atmosphere. Today we know from multiple approaches, ranging from empirical evidence to theory with supporting measurements in the lab, that atmospheric ionization governs the formation of small condensation nuclei. A higher cosmic ray flux would produce a greater degree of atmospheric ionization and would result in the formation of more small condensation nuclei. This, in turn, increases the probability that those small nuclei will become cloud condensation nuclei, producing whiter longer living clouds.

The largest variations in cosmic ray flux arise from the periodic passage of the solar system through the galactic arms. This is reflected in the exposure ages of meteorites which exhibit a roughly 145 Ma periodicity over the past billion years. And indeed, every one of these high CRF epochs corresponds to a lithologically documented ice-age episode, including the Neoproterozoic Snowball Earth. On shorter timescales, one expects a temperature oscillation to arise because of the solar systems' motion perpendicular to the galactic plane. Although the cosmic ray flux cannot be reconstructed on this shorter timescale, we do see a 32 Ma oscillation in temperature during the past 500 Ma. In the climate model presented here we propose that these oscillations are possible climate drivers.

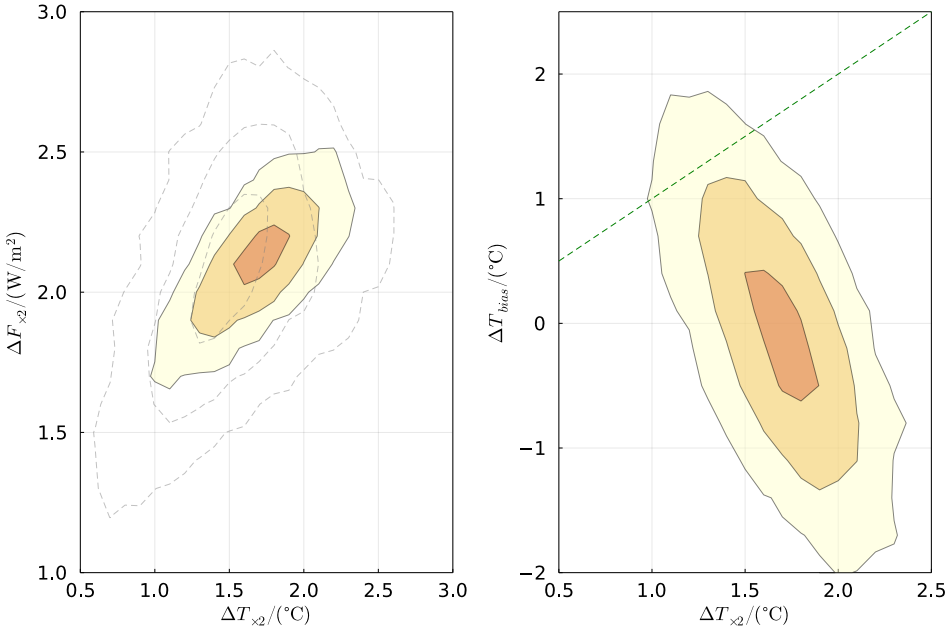

Figure 5. Left: The distribution of the radiative forcing of CO_2 doubling and climate sensitivity to CO_2 doubling mostly constrained by the model fit to both the solar brightening and CO_2 variations. Right: The distribution of the CO_2 bias parameter affecting the $\delta^{18}O$ the climate sensitivity to changes in CO_2, when other model parameters are marginalized. The dashed line corresponds to a bias for which the pH and temperature effects on $\delta^{18}O$ cancel out to give no $CO_2/\delta^{18}O$ correlation.

The last important driver that we consider is the slow, steady increase in the solar luminosity with time. This complicates the analysis because it compensates for some of the CO_2 radiative forcing which has significantly decreased over the same interval. Namely, we have to rely on the non-monotonic variations of the CO_2, if we are to find the fingerprint of either the CO_2 or the decreasing solar luminosity in the temperature model.

Armed with the above drivers, we have seen that one can build a model that explains a significant part of the temperature variations observed over the Phanerozoic. This model has unexplained residuals of only a few °C. Each of the three principal drivers (CO_2 variations, atmospheric ionization changes arising from passages through the galactic arms, and the secular increasing of the solar luminosity) provide comparable contributions of about 7-8°C to the temperature model. Interestingly however, decreases in CO_2 concentration and the increase in solar luminosity mostly cancel each other (except for the non-secular variations in CO_2). Consequently, the dominant temperature variations observed during the Phanerozoic are those due to the periodic passages of the solar system through the galactic spiral arms. The fourth important component is the vertical motion of the solar system perpendicular to the galactic plane, which is about one-third of the other contributions. These non-monotonic radiative forcings (both intrinsic and extrinsic) have relative error bars of $\sim 10\%$ or less, implying that their presence in the data is confirmed to a high statistical significance. However, some caveats should be mentioned.

Although the CO_2 forcing is detected with very high significance, there are systematic biases which we haven't considered. The CO_2 levels taken were the nominal

values of the GEOCARB-SULF model. If CO_2 levels are systematically lower/higher, then the inferred climate response to CO_2 levels should be correspondingly higher/lower than the $\Delta T_{\times 2} \approx 1.7 \pm 0.25$°C per CO_2 derived here. A second bias, mentioned above, can arise if there is an additional greenhouse gas forcing by a gas that correlates with CO_2 levels. In such a case, the climate sensitivity would be correspondingly lower. For example, the 20% increase in forcing resulting from a CH_4/CO_2 correlation, similar to that seen in ice cores, would decrease estimates of climate sensitivity to 1.35 ± 0.25°C per CO_2 doubling. We also note that this climate sensitivity includes all responses, including long-term ones such as the albedo variations associated with long term changes in the glaciations, which are generally not considered as part of the climate sensitivity on the centennial time scale.

Another interesting conclusion is that the $\delta^{18}O$ could, in principle, be used to "measure" the CO_2 radiative forcing. This is because its long-term decrease should mostly compensate for the secular solar luminosity increase to preempt any long unidirectional temperature trend over the Phanerozoic. This gives a radiative forcing which is $\sim 2/3$ of the canonical value obtained from line-by-line radiative transfer models. Thus, although we covered in this review the largest contributions to climate variations over the Phanerozoic, each one with a statistically significant fingerprint, several questions still remain open.

Acknowledgments
The authors wish to thank Christopher Scotese for the many helpful suggestions. NJS wishes to thank the generous support of the Israel Ministry of Energy.

References

Baertschi, P. (1957). *Messung und deutung relativer haufigkeitsvariationen von O-18 und C-13 in karbonatgesteinen und mineralien. schweiz.* Mineralogisches Institut der Eidg. Technischen Hochschule.

Bahcall, J. N., & Bahcall, S. (1985). The Sun's motion perpendicular to the galactic plane. *Nature*, *316*(6030), 706–708.

Bahcall, J. N., Pinsonneault, M. H., & Basu, S. (2001). Solar Models: Current Epoch and Time Dependences, Neutrinos, and Helioseismological Properties. *The Astrophysical Journal*, *555*(2), 990–1012. doi: 10.1086/321493

Berger, A. L. (1977). Support for the astronomical theory of climatic change. *Nature*, *269*(5623), 44–45. doi: 10.1038/269044a0

Berner, R. A. (2001). GEOCARB III: A revised model of atmospheric CO2 over Phanerozoic time. *American Journal of Science*, *301*(2), 182–204. doi: 10.2475/ajs.301.2.182

Berner, R. A. (2006). GEOCARBSULF: A combined model for Phanerozoic atmospheric O2 and CO2. *Geochimica et Cosmochimica Acta*, *70*(23), 5653–5664. doi: 10.1016/j.gca.2005.11.032

Boucot, A. J., Xu, C., Scotese, C. R., & Morley, R. J. (2013). *Phanerozoic Paleoclimate.* SEPM (Society for Sedimentary Geology). doi: 10.2110/sepmcsp.11

Chapman, C. R., & Morrison, D. (1994). Impacts on the Earth by asteroids and comets: Assessing the hazard. *Nature*, *367*, 33–40. doi: 10.1038/367033a0

Charney Committee. (1979). *Carbon dioxide and climate: A scientific assessment.* National Academies Press. doi: 10.17226/19856

Clapham, M. E., & Renne, P. R. (2019). Flood basalts and mass extinctions. *Annual Review of Earth and Planetary Sciences*, *47*(1), 275–303. doi: 10.1146/annurev-earth-053018-060136

Clayton, R. N., & Degens, E. T. (1959). Use of carbon isotope analyses of carbonates for differentiating fresh-water and marine sediments. *AAPG Bulletin*, *43*(4), 890–897.

Davis, W. (2017). The relationship between atmospheric carbon dioxide concentration and global temperature for the last 425 million years. *Climate*, *5*, 76.

Emiliani, C. (1954). Temperatures of Pacific bottom waters and polar superficial waters during the Tertiary. *Science*, *119*(3103), 853–855.

Enghoff, M. B., & Svensmark, H. (2008, August). The role of atmospheric ions in aerosol nucleation a review. *Atmospheric Chemistry & Physics*, *8*, 4911-4923.

Farkaš, J., Böhm, F., Wallmann, K., Blenkinsop, J., Eisenhauer, A., van Geldern, R., ... Veizer, J. (2007). Calcium isotope record of Phanerozoic oceans: Implications for chemical evolution of seawater and its causative mechanisms. *Geochimica et Cosmochimica Acta*, *71*(21), 5117–5134. doi: 10.1016/j.gca.2007.09.004

Feulner, G. (2012). The faint young Sun problem. *Reviews of Geophysics*, *50*(2), RG2006. doi: 10.1029/2011RG000375

Fichtner, H., Scherer, K., & Heber, B. (2006). A criterion to discriminate between solar and cosmic ray forcing of the terrestrial climate. *Atmospheric Chemistry & Physics Discussions*, *6*, 10811-10836.

Frakes, L. A., Francis, J. E., & Syktus, J. I. (1992). *Climate modes of the Phanerozoic*. Cambridge University Press.

Genthon, G., Barnola, J. M., Raynaud, D., Lorius, C., Jouzel, J., Barkov, N. I., ... Kotlyakov, V. M. (1987). Vostok ice core: climatic response to CO2 and orbital forcing changes over the last climatic cycle. *Nature*, *329*(6138), 414–418. doi: 10.1038/329414a0

Goddéris, Y., Donnadieu, Y., & Pohl, A. (2021). "The Phanerozoic Climate". In G. Ramstein, A. Landais, N. Bouttes, P. Sepulchre, & A. Govin (Eds.), *Paleoclimatology* (pp. 359–383). Cham: Springer International Publishing. doi: 10.1007/978-3-030-24982-3_27

Gough, D. O. (1981). Solar interior structure and luminosity variations. *Sol. Phys.*, *74*(1), 21–34. doi: 10.1007/bf00151270

Grossman, E. L. (2012a). Applying oxygen isotope paleothermometry in deep time. *The Paleontological Society Papers*, *18*, 39–68.

Grossman, E. L. (2012b). Oxygen isotope stratigraphy. In *The geologic time scale* (pp. 181–206). Elsevier. doi: 10.1016/b978-0-444-59425-9.00010-x

Haigh, J. D. (1994). The Role of Stratospheric Ozone in Modulating the Solar Radiative Forcing of Climate. *Nature*, *370*, 544. doi: 10.1038/370544a0

Haigh, J. D., Blackburn, M., & Day, R. (2005). The Response of Tropospheric Circulation to Perturbations in Lower-Stratospheric Temperature. *Journal of Climate*, *18*, 3672-3685. doi: 10.1175/JCLI3472.1

Hays, J. D., Imbrie, J., & Shackleton, N. J. (1976). Variations in the Earth's Orbit: Pacemaker of the Ice Ages. *Science*, *194*(4270), 1121–1132. doi: 10.1126/science.194.4270.1121

Holmberg, J., & Flynn, C. (2000). The local density of matter mapped by Hipparcos. *Monthly Notices of the Royal Astronomical Society*, *313*(2), 209–216.

Howard, D., Shaviv, N. J., & Svensmark, H. (2015). The solar and southern oscillation components in the satellite altimetry data. *Journal of Geophysical Research: Space Physics*, *120*(5), 3297–3306. (2014JA020732) doi: 10.1002/2014JA020732

Hoyle, F. (1958). Remarks on the computation of evolutionary tracks. *Ricerche Astronomiche*, *5*, 223.

Imbrie, J., Boyle, E. A., Clemens, S. C., Duffy, A., Howard, W. R., Kukla, G., ... Toggweiler, J. R. (1992). On the Structure and Origin of Major Glaciation Cycles 1. Linear Responses to Milankovitch Forcing. *Paleoceanography*, *7*(6), 701–738. doi: 10.1029/92pa02253

IPCC. (2013). Summary for policymakers [Book Section]. In T. Stocker et al. (Eds.), *Climate change 2013: The physical science basis. contribution of working group i to the fifth assessment report of the intergovernmental panel on*

climate change (p. 1–30). Cambridge, United Kingdom and New York, NY, USA: Cambridge University Press. doi: 10.1017/CBO9781107415324.004

Kampschulte, A., & Strauss, H. (2004). The sulfur isotopic evolution of Phanerozoic seawater based on the analysis of structurally substituted sulfate in carbonates. *Chemical Geology*, *204*(3-4), 255–286.

Kasting, J. F. (1993). Earth's Early Atmosphere. *Science*, *259*(5097), 920-926. doi: 10.1126/science.259.5097.920

Kirkby, J., Curtius, J., Almeida, J., Dunne, E., Duplissy, J., Ehrhart, S., ... others (2011). Role of sulphuric acid, ammonia and galactic cosmic rays in atmospheric aerosol nucleation. *Nature*, *476*(7361), 429–433.

Kopp, R. E., Kirschvink, J. L., Hilburn, I. A., & Nash, C. Z. (2005). The Paleoproterozoic snowball earth: A climate disaster triggered by the evolution of oxygenic photosynthesis. *Proceedings of the National Academy of Sciences*, *102*(32), 11131–11136. doi: 10.1073/pnas.0504878102

Köppen, W., & Berlin, A. W. (1924). Die Klimate der geologischen Vorzeit. Berlin (Gebrüdr Borntraeger).

Kuhn, W. R., & Kasting, J. F. (1983). Effects of increased CO2 concentrations on surface temperature of the early earth. *Nature*, *301*, 53-55. doi: 10.1038/301053a0

Lavielle, B., Marti, K., Jeannot, J.-P., Nishiizumi, K., & Caffee, M. (1999). The ^{36}Cl ^{36}Ar ^{40}K ^{41}K records and cosmic ray production rates in iron meteorites. *Earth and Planetary Science Letters*, *170*(12), 93 - 104. doi: 10.1016/S0012-821X(99)00099-0

Lee, H., & Smith, A. K. (2003). Simulation of the combined effects of solar cycle, quasi-biennial oscillation, and volcanic forcing on stratospheric ozone changes in recent decades. *Journal of Geophysical Research (Atmospheres)*, *108*, 4049. doi: 10.1029/2001JD001503

McInerney, F. A., & Wing, S. L. (2011). The Paleocene-Eocene Thermal Maximum: A Perturbation of Carbon Cycle, Climate, and Biosphere with Implications for the Future. *Annual Review of Earth and Planetary Sciences*, *39*(1), 489–516. doi: 10.1146/annurev-earth-040610-133431

Milankovitch, M. (1920). Theorie Mathematique des Phenomenes Thermiques produits par la Radiation Solaire. Gauthier-Villars, Paris, 340 p.

Muller, R. A. (1997). Glacial cycles and astronomical forcing. *Science*, *277*(5323), 215–218. doi: 10.1126/science.277.5323.215

Myhre, G., Highwood, E. J., Shine, K. P., & Stordal, F. (1998). New estimates of radiative forcing due to well mixed greenhouse gases. *Geophysical Research Letters*, *25*(14), 2715–2718. doi: 10.1029/98gl01908

Pisias, N. G., & Shackleton, N. J. (1984). Modelling the global climate response to orbital forcing and atmospheric carbon dioxide changes. *Nature*, *310*(5980), 757–759. doi: 10.1038/310757a0

Pollack, J. B. (1991). Kuiper prize lecture: Present and past climates of the terrestrial planets. *Icarus*, *91*(2), 173-198. doi: 10.1016/0019-1035(91)90017-N

Pope, K. O., Baines, K. H., Ocampo, A. C., & Ivanov, B. A. (1994). Impact winter and the Cretaceous/Tertiary extinctions: Results of a Chicxulub asteroid impact model. *Earth and Planetary Science Letters*, *128*(3), 719-725. doi: https://doi.org/10.1016/0012-821X(94)90186-4

Prokoph, A., Shields, G., & Veizer, J. (2008). Compilation and time-series analysis of a marine carbonate δ18O, δ13C, 87Sr/86Sr and δ34S database through Earth history. *Earth-Science Reviews*, *87*(3-4), 113–133.

Ringwood, A. E. (1961). Changes in solar luminosity and some possible terrestrial consequences. *Geochimica et Cosmochimica Acta*, *21*(3-4), 295-296. doi: 10.1016/S0016-7037(61)80064-1

Royer, D. L., Berner, R. A., Montañez, I. P., Tabor, N. J., Beerling, D. J., et al. (2004). CO_2 as a primary driver of Phanerozoic climate. *GSA today*, *14*(3),

4–10.

Royer, D. L., Donnadieu, Y., Park, J., Kowalczyk, J., & Godderis, Y. (2014). Error analysis of CO2 and O2 estimates from the long-term geochemical model GEOCARBSULF. *American Journal of Science*, *314*(9), 1259–1283. doi: 10.2475/09.2014.01

Ruddiman, W. F. (2006). Ice-driven CO_2 feedback on ice volume. *Climate of the Past*, *2*(1), 43–55. Retrieved from `https://cp.copernicus.org/articles/2/43/2006/` doi: 10.5194/cp-2-43-2006

Sagan, C., & Mullen, G. (1972). Earth and Mars: Evolution of Atmospheres and Surface Temperatures. *Science*, *177*(4043), 52–56. doi: 10.1126/science.177.4043.52

Schwarzschild, M. (1958). *Structure and evolution of stars.* Princeton University Press.

Scotese, C. R. (2016). Paleomap paleoatlas for gplates and the paleodata plotter program. *PALEOMAP Project*. Retrieved from `http://www.earthbyte.org/paleomap-paleoatlas-for-gplates/`

Scotese, C. R. (2021). An atlas of Phanerozoic paleogeographic maps: The seas come in and the seas go out. *Annual Review of Earth and Planetary Sciences*, *49*(1), 679-728. doi: 10.1146/annurev-earth-081320-064052

Scotese, C. R., Song, H., Mills, B. J., & van der Meer, D. G. (2021). Phanerozoic paleotemperatures: The earth's changing climate during the last 540 million years. *Earth-Science Reviews*, *215*, 103503. doi: 10.1016/j.earscirev.2021.103503

Shaviv, N. J. (2002). Cosmic Ray Diffusion from the Galactic Spiral Arms, Iron Meteorites, and a Possible Climatic Connection. *Phys. Rev. Lett.*, *89*(5), 051102. doi: 10.1103/PhysRevLett.89.051102

Shaviv, N. J. (2003a). The spiral structure of the Milky Way, cosmic rays, and ice age epochs on Earth. *New Astronomy*, *8*, 39-77. doi: 10.1016/S1384-1076(02)00193-8

Shaviv, N. J. (2003b). Toward a solution to the early faint Sun paradox: A lower cosmic ray flux from a stronger solar wind. *Journal of Geophysical Research (Space Physics)*, *108*(A12), 1437. doi: 10.1029/2003JA009997

Shaviv, N. J. (2005). On climate response to changes in the cosmic ray flux and radiative budget. *Journal of Geophysical Research (Space Physics)*, *110*(A9), 8105. doi: 10.1029/2004JA010866

Shaviv, N. J. (2008). Using the oceans as a calorimeter to quantify the solar radiative forcing. *Journal of Geophysical Research (Space Physics)*, *113*(A12), 11101. doi: 10.1029/2007JA012989

Shaviv, N. J. (2016). *A kinematic spiral arm shock signature: "Ringing" in the vertical motion of stars.* (arXiv:1606.02595)

Shaviv, N. J., & Veizer, J. (2003). A Celestial Driver of Phanerozoic Climate? *GSA Today*, *13*, (7) 4–11. doi: 10.1130/1052-5173(2003)0132.0.CO;2

Song, H., Kemp, D. B., Tian, L., Chu, D., Song, H., & Dai, X. (2021, August). Thresholds of temperature change for mass extinctions. *Nature Communications*, *12*(1). Retrieved from `https://doi.org/10.1038/s41467-021-25019-2` doi: 10.1038/s41467-021-25019-2

Song, H., Wignall, P. B., Song, H., Dai, X., & Chu, D. (2019). Seawater temperature and dissolved oxygen over the past 500 million years. *Journal of Earth Science*, *30*(2), 236–243. doi: 10.1007/s12583-018-1002-2

Steuber, T., & Veizer, J. (2002). Phanerozoic record of plate tectonic control of seawater chemistry and carbonate sedimentation. *Geology*, *30*(12), 1123–1126.

Stothers, R. B. (1998). Galactic disc dark matter, terrestrial impact cratering and the law of large numbers. *Monthly Notices of the Royal Astronomical Society*, *300*(4), 1098–1104.

Svensmark, H., Bondo, T., & Svensmark, J. (2009). Cosmic ray decreases affect at-

mospheric aerosols and clouds. *Gephysical Research Letters*, *36*, 15101. doi: 10 .1029/2009GL038429

Svensmark, H., Enghoff, M. B., & Pedersen, J. O. P. (2013). Response of cloud condensation nuclei (> 50 nm) to changes in ion-nucleation. *Physics Letters A*, *377*, 2343-2347. doi: 10.1016/j.physleta.2013.07.004

Svensmark, H., Enghoff, M. B., Shaviv, N. J., & Svensmark, J. (2017). Increased ionization supports growth of aerosols into cloud condensation nuclei. *Nature Communications*, *8*(1), 2199. doi: 10.1038/s41467-017-02082-2

Svensmark, H., & Friis-Christensen, E. (1997). Variation of cosmic ray flux and global cloud coverage - a missing link in solar-climate relationships. *Journal of Atmospheric and Solar-Terrestrial Physics*, *59*(11), 1225-1232.

Svensmark, H., Pedersen, J. O. P., Marsh, N. D., Enghoff, M. B., & Uggerhøj, U. I. (2007). Experimental evidence for the role of ions in particle nucleation under atmospheric conditions. *Royal Society of London Proceedings Series A*, *463*, 385-396. doi: 10.1098/rspa.2006.1773

Svensmark, J., Enghoff, M. B., Shaviv, N. J., & Svensmark, H. (2016). The response of clouds and aerosols to cosmic ray decreases. *Journal of Geophysical Research: Space Physics*, 8152–8181. (2016JA022689) doi: 10.1002/2016JA022689

Ulrich, R. K. (1975). Solar Neutrinos and Variations in the Solar Luminosity. *Science*, *190*(4215), 619-624.

Urey, H. C., Lowenstam, H. A., Epstein, S., & McKinney, C. R. (1951). Measurement of paleotemperatures and temperatures of the Upper Cretaceous of England, Denmark, and the southeastern United States. *Geological Society of America Bulletin*, *62*(4), 399–416.

Veizer, J., Ala, D., Azmy, K., Bruckschen, P., Buhl, D., Bruhn, F., ... Strauss, H. (1999). $^{87}Sr/^{86}Sr$, $\delta^{13}C$ and $\delta^{18}O$ evolution of Phanerozoic seawater. *Chemical Geology*, *161*(1-3), 59–88. doi: 10.1016/s0009-2541(99)00081-9

Veizer, J., Godderis, Y., & François, L. M. (2000). Evidence for decoupling of atmospheric CO2 and global climate during the Phanerozoic eon. *Nature*, *408*(6813), 698–701.

Veizer, J., & Prokoph, A. (2015). Temperatures and oxygen isotopic composition of Phanerozoic oceans. *Earth-Science Reviews*, *146*, 92–104. doi: 10.1016/j .earscirev.2015.03.008

Vellekoop, J., Esmeray-Senlet, S., Miller, K. G., Browning, J. V., Sluijs, A., van de Schootbrugge, B., ... Brinkhuis, H. (2016). Evidence for Cretaceous-Paleogene boundary bolide "impact winter" conditions from New Jersey, USA. *Geology*, *44*(8), 619-622. doi: 10.1130/G37961.1

Vérard, C., & Veizer, J. (2019). On plate tectonics and ocean temperatures. *Geology*, *47*(9), 881–885. doi: 10.1130/g46376.1

Vollstaedt, H., Eisenhauer, A., Wallmann, K., Böhm, F., Fietzke, J., Liebetrau, V., ... Veizer, J. (2014). The Phanerozoic δ88/86Sr record of seawater: New constraints on past changes in oceanic carbonate fluxes. *Geochimica et Cosmochimica Acta*, *128*, 249–265. doi: 10.1016/j.gca.2013.10.006

Zeebe, R. E. (1999). An explanation of the effect of seawater carbonate concentration on foraminiferal oxygen isotopes. *Geochimica et Cosmochimica Acta*, *63*(13), 2001-2007. doi: 10.1016/S0016-7037(99)00091-5

Zeebe, R. E. (2001). Seawater pH and isotopic paleotemperatures of Cretaceous oceans. *Palaeogeography, palaeoclimatology, palaeoecology*, *170*(1-2), 49–57.